COBEM 2023 27TH INTERNATIONAL CONGRESS OF MECHANICAL ENGENEERING

ABCM Brazilian Society of Mechanical Sciences and Engineering
27th ABCM International Congress of Mechanical Engineering
December 04-08, 2023, Florianópolis-SC, Brazil

COB-2023-XXXX
NON-LINEAR ELECTRICAL SUBMERSIBLE PUMP MODEL FOR MODEL PREDICTIVE CONTROL CONSIDERING VISCOUS EFFECTS

Mauricio Barrios Castellanos
Alberto Luiz Serpa
Department of Computational Mechanics, School of Mechanical Engineering, University of Campinas (UNICAMP)
mauricio.bc.89@gmail.com, alserpa@unicamp.br

Abstract. *Electric Submersible Pumps (ESPs) are critical equipment for the artificial lift and transportation of viscous fluids. ESPs also work in severe conditions, including abrasion, gas, and emulsion, requiring continuous monitoring and control. Model Predictive Control (MPC) is a process control approach that can reduce energy consumption, keeping the operation safe within operational limits. This paper presents a non-linear ESP model for MPC based on the Hammerstein-Wiener modeling strategy. The proposed model presents a simplified solution for pumping dynamics considering the changes in fluid viscosity, enabling safe and continuous operation.*
The experimental arrangement consists of an 8-stage ESP operating with oil. The experiments were in steady-state and transient-state. The experimental procedure consists of varying pump rotation and choke valve aperture. The pump rotation varied from 1000 to 3500 rpm in steps between 0 and 300 rpm. The choke valve opening varied from 19 to 100% of in steps between 0 and 1%. The fluid's viscosity in the experiments was monitored, varying between 70 to 250 cP.
This paper proposes a non-linear model that considers the viscosity effects of the fluid in the system dynamics. The model formulation involves a non-linear model in which the dynamic state-space model (DSSM) inputs are the outputs of a non-linear steady-state model (SSM). The SSM considered the pump and the downstream elements, including the choke valve. The proposed model was fitted and validated using experimental data. A simulation comparing the model and the experimental setup behavior shows errors below 5% between prediction and plant in at least 80% of the simulation.

Keywords: *Non-Linear Model Predictive Control, Electrical Submersible Pump, Dynamical Model, Fluid Mechanics*

1. INTRODUCTION

Centrifugal pumps consist of a moving part and a static one. The moving part is a rotor that supplies kinetic energy to the fluid, transporting it from the center of the rotor to the outside through centrifugal force. The static part is a casing with two geometric configurations: a diffuser in multi-stage pumps, responsible for transforming kinetic energy into potential pressure energy and supplying the fluid to the next stage, or a volute in one-stage pumps.

The pressure developed in centrifugal pumps is correlated with the volume of liquid transported, making them suitable for high-flow and low-pressure applications. While water viscosity is approximately one cP under normal conditions, ESP can handle heavy oils with viscosities between one hundred and one thousand cP. Furthermore, the fluid extracted from the well is an inhomogeneous mixture of oil, water, gas, sand, and sediment.

An ESP system model should consider the following aspects: well fluid properties, well temperature profile, ESP equipment performance, reservoir flow performance, pump depth, tubing and casing size, pressure in the pipe, and the flow rate. The calculations behind the performance simulations of ESP-based well systems iteratively solve a set of algebraic and differential equations of conservation of mass, momentum, and energy. For multiphase ESP systems, the computation time for converging calculations is not negligible (Denney *et al.*, 2013).

Kullick and Hackl (2017) provided a parametric model of an ESP system, including modeling for the electrical, mechanical, and hydraulic systems. The model is a state-of-spaces as the basis for developing model-based predictive maintenance, state observers, and control algorithms.

The information provided by the dynamic model of the system is essential in the controllers design. The ESP hydrodynamic behavior corresponds to a turbomachine. Kullick and Hackl (2017) proposed a parametric model in ESP modeling based on the research conducted by Saito (1982) and Dazin *et al.* (2007) for transients turbomachinery speeds.

The models proposed by Dazin *et al.* (2007) and Saito (1982) were based on theoretical analyzes of the turbomachine fast transients and the study of incompressible fluid mechanics equations applied to a rotor, including the internal torque, internal power, and impeller pressure during transitory periods. Saito (1982) presented the equations of dynamic behavior as a function of the variation in rotation over time and the variation in the surrounding flow. Dazin *et al.* (2007) added the effects produced by velocity profiles on the pump impeller.

The ESP system comprises different subsystems of electrical, mechanical, and hydraulic types. Thorsen and Dalva

(2001) developed kinematic models for electrical and mechanical ESP systems to predict transient voltages on shafts, and electrical and mechanical conditions at startup. Janevska (2013) presented a state-space pump model consisting of a centrifugal pump driven by an asynchronous three-phase electric motor and pumping from a constant-level water tank.

The centrifugal pump analytical models consider a volute-rotor pump operating in a one-phase flow regime. However, ESPs are diffuser-rotor multi-stage pumps that operate in most liquid-gas and liquid-liquid multiphase viscous flows. For this reason, Machine Learning (ML) models become attractive in the ESP identification of two-phase systems.

Machine Learning is a parameter adjustment process. An input-output data set adjusts the algorithm parameters, generating a system model. Essential efforts were in developing data-driven ML models to monitor ESP conditions. The ML methods used for modeling ESP systems include Support Vector Machines (SVM) (Jimenez *et al.*, 2016; Ricardo *et al.*, 2018; Jimenez, 2019) and Artificial Neural Networks (ANN) (Pineda, 2016; Bukhtoyarov *et al.*, 2019).

Models based on ML require large amounts of data. In the ideal scenario, a data-driven approach would require sampling all possible combinations of components from an ESP system (Lastra, 2019). The data-based conventional learning models have no relation with the physical phenomena (Thornhill *et al.*, 2009; Adesanwo *et al.*, 2019). Although the data comes from a physical process, phenomenological aspects are usually not considered. Therefore, the obtained model is a mathematical model that approximates a particular system, but this may not work well for other similar systems.

An alternative to ML models is the hybrid model, which considers the ESP system's phenomenological aspects in ML-based methodologies (Adesanwo *et al.*, 2019; Lastra, 2019).

Considering the predominant physical phenomenon, control strategies based on MPC allow confident operation in standard intervals. Recently, strategies based on MPC were proposed, including flow dynamics in pipes and correction by highly viscous fluids (Pavlov *et al.*, 2014; Krishnamoorthy *et al.*, 2016; De Delou *et al.*, 2019).

Pavlov *et al.* (2014) presented a dynamic model of an oil well equipped with ESP, developed for a Model Predictive Control (MPC). This model proposes MPC targets and constraints in an ESP-well system considering the transient variation presented in the pipes due to the variations in flow rate. Pavlov *et al.* (2014) studied the case of a pump operating with a low viscous fluid, excluding the transient effects in the pump system.

Krishnamoorthy *et al.* (2016) extended the Pavlov *et al.* (2014) model considering each ESP stage as an independent volume control. Each volume control consists of a model of a centrifugal pump. The model considers the ESP head variation as a function of a rotational speed based on the pump affinity laws and corrected by a viscosity correction factor. Krishnamoorthy *et al.* (2016) modeled the choke valve as a flow through a restriction in which the flow coefficient varied based on the choke valve opening. The system dynamics assume the flow variation in pipes. The data to test the model reaches from an ESP-well simulator.

De Delou *et al.* (2019) proposed a multi-model linear MPC (MMPC) based on the model proposed by Pavlov *et al.* (2014). The model's target was the control of inlet pressure reducing power consumption. The MMPC consists of the transition between linear models based on a homotopy function of the choke valve opening.

This study proposed a non-linear steady-state modeling coupled with a linear dynamical model for an ESP system based on the Hammerstein-Wiener approach (Greblicki and Pawlak, 1986, 1994). The remainder of this work is organized in Section 2, which includes the experimental facilities and the procedure. The model formulation is presented in Section 3. Section 4 compares the model with different operational points, discussing and comparing its results. The conclusions are presented in Section 5. Finally, Section 7 and Section 6 include the acknowledgments and references, respectively.

2. MATERIALS AND METHODS

2.1 Experimental setup

The principal equipment is an eight stages ESP, each with a 7-blade rotor of 108 [mm] diameter. The experimental bench includes the two-screw pump, the choke valve, variable speed drives (VSD), the heat exchanger subsystem, auxiliary valves, and instrumentation. The fluid is mineral oil. The oil's dynamic viscosity changes with temperature variations, and a rheometer HAAKE MARS III characterizes it.

Figure 1 presents the experimental bench and oil viscosity variation with temperature. Figure 1a shows the experimental layout. The fluid circuit begins with the oil pumped from the tank by the two-screw pump. The oil flows through the heat exchanger and Coriolis meter. Subsequently, the oil flows through the ESP, the choke valve, and returns to the tank, closing the loop. The VSD-1 and the VSD-2 regulate the rotation of the two-screw pump and ESP, respectively. The heat exchanger has an independent water circuit composed of a heater, a water tank, and a chiller. The water is regulated to maintain the ESP's intake temperature T_{in} at a desired value.

Figure 1b presents the behavior of dynamical viscosity with the temperature given by the rheometer. Table 1 presents a detailed specification of the principal equipment and the instrumentation.

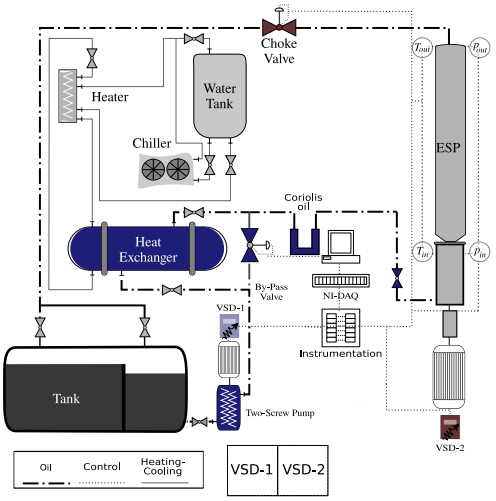

(a) Experimental layout

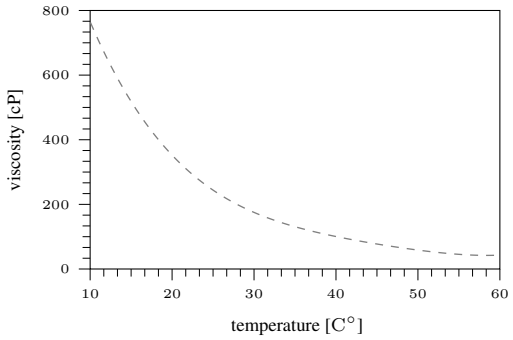

(b) Oil Dynamic viscosity measured by rheometer HAAKE MARS III

Figure 1: Experimental layout and oil viscosity variations.

Table 1: Equipment and sensors specification.

Device	Model	Specification	
Two-screw Pump	NETZSCH	Motor WEG	45 [kW], 1775 [RPM] 60 [Hz]
ESP	Baker Hughes P100LS	Motor WEG	37 [kW], 3555 [RPM] 60 [Hz]
Choke valve	Fisher 657	Glob valve	
VSD-1	CFW 700 WEG	Vectrue inverter	
VSD-2	CFW 09 WEG	Vectrue inverter	
Tank	Intelfibra	Capacity 12000 [L]	
Heat Exchanger	FYTERM T3480	Shell and tube	
Heater	TMR-M-18-380/C	Mecalor device	
Chiller	MSA-60-CA-380/C	Mecalor device	
Flow meters	MicroMotion F300S355	$0 - 100$ [m^3/h]	Uncertainty 0.2% of value
Temperature sensors	ECIL PT100	$0 - 100$ [°C]	Uncertainty 0.07% of value
Pressure transducers	Emerson Rosemount 2088	$0 - 20$ [bar]	Uncertainty 0.07% of full scale
Encoder	Minipa MDT-2238A	$0 - 166$ [Hz]	Uncertainty 0.05% of full scale

2.2 Experimental procedure

First, the two-screw rotation is fixed in a given value, with a choke valve opening y at 100% and ESP rotation ω at 0 rpm. The choke valve is closed until the input pressure p_{in} exceeds 3 bar. Then, follow the next procedure until ω reaches 3500 rpm:

1. Increase the ESP rotation randomly with a maximum difference of 300 rpm and wait 10 seconds until the system becomes in a steady-state;
2. The choke valve is closed in a random step with a maximum of 2 and wait 10 seconds until the system becomes in a steady-state;
3. If the p_{in} is below 3 bar, repeat, go to step 2; otherwise, go to step 1.

Subsequently, the process is inverted, decreasing ω and opening the choke valve with the same p_{in} restriction. The experimental test is unconsidered if the input pressure is below 0 bar or the p_{in} is greater than the output pressure p_{out}. Figure 2 presents an example of the experimental test where the pump head h is calculated like

$$h = \frac{p_{out} - p_{in}}{\rho g}, \tag{1}$$

with ρ as the oil density and g as the gravitational acceleration constant.

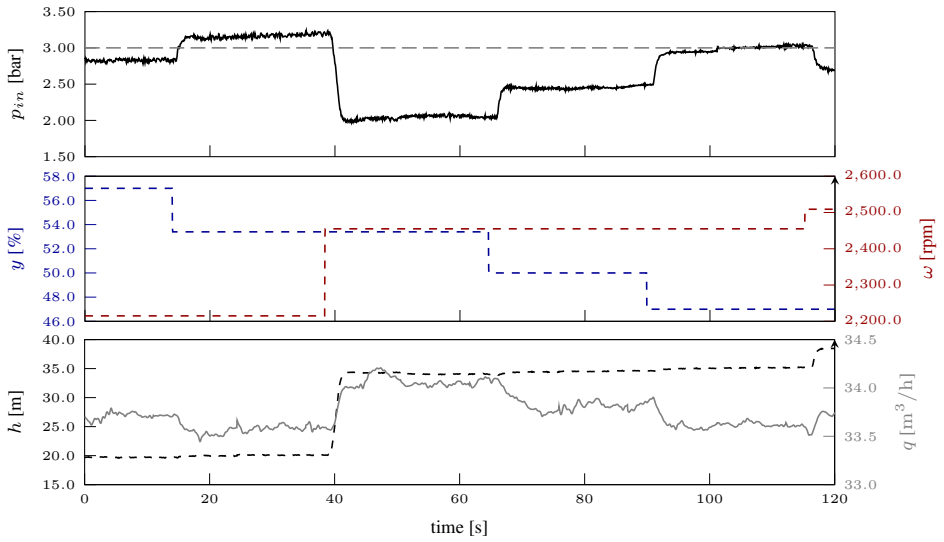

Figure 2: Transient test example

3. METHODOLOGY

3.1 Model system approach

Dazin *et al.* (2007) describe the dynamical model of a pump by the following equation:

$$h = C_1\omega^2 + C_2 q\omega - C_3 q^2 + C_4\frac{d\omega}{dt} - C_5\frac{dq}{dt}. \tag{2}$$

Here, h corresponds to the pump head defined in Equation 1, q is the flow rate across the pump and ω is the pump's rotational speed. The parameters C_1 to C_5 are considered constants and depend on the geometry of the pump when the working fluid is water.

When the fluid is a viscous fluid, such as oil, the parameter C_3 varies with changes in viscosity μ and can be described by the equation formulated by Biazussi (2014), i.e.,

$$C_3 = K_1 + K_2\frac{1}{Re} + K_3\left(\frac{1}{Re}\right)^n \qquad \text{with} \qquad Re = \frac{4\rho q}{\mu D_p}. \tag{3}$$

Re is the Reynolds number depending on the pump rotor diameter D_p of the ESP, and the parameters K_1, K_2, and K_3 are adjustable for each pump.

The above equations exhibit high non-linearities in the dynamical model. However, we can consider that the constants C_4 and C_5 depend only on the geometrical and construction factors of the pump. In that case, the non-linearities are only in the steady-state terms of the differential equation.

To account for this behavior of the pump system, we propose a Hammerstein-Wiener approach according to Greblicki and Pawlak (1986, 1994) applied to the pumping system modeling. The model formulation involves a non-linear model where the inputs of the dynamic state-of-space model (DSSM) are the outputs of a non-linear steady-state model (SSM).

An ESP system's simplified point of view consists of piping, a pump (ESP), a choke valve, a tank to store the fluid, and a reservoir in which the pressure changes with the flow rate variation. Figure 3a exemplifies the system.

The proposed approach divides the SSM into the reservoir model and ESP steady-state model (ESP SSM). The reservoir model correlates the p_{in}, and the system flow rate q. The ESP SSM correlates the output pressure p_{out}, head h, and flow rate q of the ESP as a function of ω and y and includes the ESP and the ESP upstream elements. Figure 3b schematizes the proposed model.

The system's manipulated variables (MV) are y and ω. The inputs ($\boldsymbol{u}$) and outputs ($\boldsymbol{v}$) of the ESP SSM are

$$\boldsymbol{u} = \begin{bmatrix} u_1 \\ u_2 \end{bmatrix} = \begin{bmatrix} y \\ \omega \end{bmatrix}, \qquad \boldsymbol{v} = \begin{bmatrix} v_1 \\ v_2 \end{bmatrix} = \begin{bmatrix} h^{(ss)} \\ p_{out}^{(ss)} \end{bmatrix}. \tag{4}$$

$h^{(ss)}$ and $p_{out}^{(ss)}$ correspond to the steady-state head and output pressure predictions, respectively. The DDSM predicts

(a) Simplified ESP system

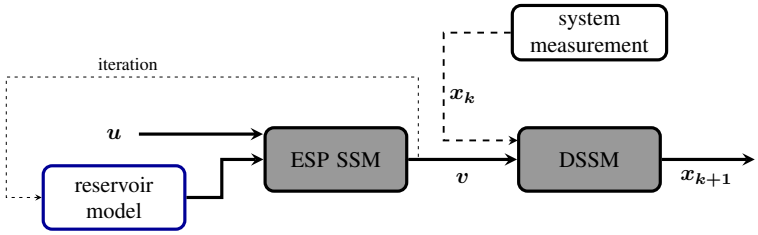

(b) Hammerstein-Wiener approach

Figure 3: Hammerstein-Wiener approach for an ESP system

the behavior of the output pressure $p_{out}^{(dyn)}$ and head $h^{(dyn)}$ as a function of $\boldsymbol{v}$, and the system measurement of head h and output pressure p_{out}, as presented in the sequence.

$$\boldsymbol{x}_k = \begin{bmatrix} x_1 \\ x_2 \end{bmatrix} = \begin{bmatrix} h \\ p_{out} \end{bmatrix}; \qquad \boldsymbol{x}_{k+1} = \begin{bmatrix} v_1 \\ v_2 \end{bmatrix} = \begin{bmatrix} h^{(dyn)} \\ p_{out}^{(dyn)} \end{bmatrix}. \tag{5}$$

3.2 Steady-state model

Considering the steady-state terms of equations 2 and 3, the $h^{(ss)}$ as function of the flow rate in steady-state $q^{(ss)}$, viscosity μ and density ρ of fluid is given by

$$h^{(ss)} = k_1\omega^2 - k_2\omega q^{(ss)} - \left(k_3 + k_4\frac{\mu}{\rho q^{(ss)}} + k_5\left(\frac{\mu}{\rho q^{(ss)}}\right)^n\right) {q^{(ss)}}^2. \tag{6}$$

Here, k_1 and k_2 terms consider the ideal Euler equation and the pressure losses related to secondary flow, recirculation, and inertial losses. k_3 and k_4 terms correspond to friction losses, which depend on the fluid viscosity, and k_5 depends on recirculation, inertial, secondary and localized losses.

The output pressure $p_{out}^{(ss)}$ is the sum of pressure losses in the choke valve given by

$$\Delta p_{choke} = {q^{(ss)}}^2 \rho \left(cv(y)^{-2}\right), \tag{7}$$

and the pressure losses in the upstream pipe correspond to

$$\Delta p_{up} = f(q^{(ss)}, \mu, \rho, d)\frac{\rho}{2}\frac{l}{d}\left(\frac{4q^{(ss)}}{\pi d^2}\right)^2. \tag{8}$$

Here, d is the internal diameter of the upstream pipe. l is the equivalent length of the output pipe, considering the minor losses caused by pipe inlets, exits elbows, and fully open auxiliary valves (Robert W. Fox *et al.*, 2020). For the experimental bench output pipe, d is 93 mm, and l is 52.858 m. The friction factor in the output pipe f is function of flow rate $q^{(ss)}$, viscosity μ, density ρ, and pipe diameter d. For laminar flow with Reynolds number Re below the 2300 f is $64/Re$. Otherwise, f is calculated with the Haaland equation for cast iron (Robert W. Fox *et al.*, 2020).

A choke valve's flow coefficient $cv(y)$ correlates the pressure losses Δp_{choke} and the flow rate across the valve. The $cv(y)$ varies with the choke opening y. The variation of $cv(y)$ depends on design criteria. In the experimental bench, the $cv(y)$ design criteria corresponds to a percentage criteria and can be approximated like a sigmoid function (de Campos and Teixeira, 2010). The $cv(y)$ is adjusted to

$$cv(y) = m_2\left(\left(1 + e^{-m_1(y-y_0)}\right)^{-1} + cv_0\right), \tag{9}$$

where m_1, m_2, cv_0, and y_0 are constants, which describes the flow coefficient as a sigmoid function.

Combining equations 7 and 8, the ESP output pressure in steady-state can be written as

$$\begin{aligned} p_{out}^{(ss)} &= \Delta p_{choke} + \Delta p_{up} \\ p_{out}^{(ss)} &= \frac{{q^{(ss)}}^2 \rho}{cv(y)^2} + f(q^{(ss)}, \mu, \rho, d)\frac{\rho}{2}\frac{l}{d}\left(\frac{4q^{(ss)}}{\pi d^2}\right)^2. \end{aligned} \tag{10}$$

3.3 Reservoir model

The reservoir is a non-linear equation where the flow rate ($q^{(ss)}$) and the ESP input pressure ($p_{in}^{(ss)}$) are correlated. In laboratory experiments, the input pressure depends on the mechanical restriction of a two-screw pump. The flow rate in a two-screw pump varied with the rotational speed of the two-screw pump ω_s and the sleep factor S by

$$q^{(ss)} = vc_s\omega_s - S(\mu)\Delta p_s, \tag{11}$$

where vc_s is the volumetric capacity of the positive displacement pump, Δp_b is the gain pressure of the two-screw pump, and S is a sleep factor that varies as a function of viscosity μ (Karassik *et al.*, 1976).

The sleep factor model proposed consists of the function

$$S(\mu) = \omega_b \frac{m_s}{\mu} + b_s, \tag{12}$$

where m_s and b_s are adjustable parameters.

The input pressure in the ESP in steady-state corresponds to the two-screw gain pressure Δp_s minus the pressure losses in the pipe and the auxiliary elements, i.e.,

$$p_{in}^{(ss)} = \Delta p_s - f(q^{(ss)}, \mu, \rho, d)\frac{\rho}{2}\frac{l_{eq}}{d}\left(\frac{4q^{(ss)}}{\pi d^2}\right)^2. \tag{13}$$

Here, the friction factor is the same as in the output pipe, and the l_{eq} includes the major and minor loss in the downstream line and is considered 147.93 [m].

Combining equations 11 and 13, the reservoir model equation for the experimental bench is

$$q^{(ss)} = vc_s\omega_s - S(\mu)\left(p_{in}^{(ss)} + f(q^{(ss)}, \mu, \rho, d)\frac{\rho}{2}\frac{l_{eq}}{d}\left(\frac{4q^{(ss)}}{\pi d^2}\right)^2\right). \tag{14}$$

3.4 Dynamical model

The proposed dynamical model can be represented as a linear state-of-spaces model, i.e.,

$$\dot{\boldsymbol{x}}_k = \boldsymbol{A}\boldsymbol{x}_k + \boldsymbol{B}\boldsymbol{v}_k, \tag{15}$$

$$\dot{\boldsymbol{x}}_k = \frac{\boldsymbol{x}_{k+1} - \boldsymbol{x}_k}{T}, \tag{16}$$

$$\boldsymbol{x}_{k+1} = \boldsymbol{x}_k + \dot{\boldsymbol{x}}_k T \tag{17}$$

Here, T is the sampling time between the sample k and $k+1$, $\boldsymbol{v}$ represents the inputs, and $\boldsymbol{x}$ represents the outputs of the DSSM defined in equations 4 and 5. $\boldsymbol{A}$ is the state matrix and $\boldsymbol{B}$ is the input matrix.

3.5 Model fit and test

The data fit corresponds to 50% of the randomly selected data; the rest is used to test the model. Figure 4 presents the data distribution as a function of process variables.

Steady-state equations parameters k_1, k_2, k_3, k_4, and k_5 are adjusted by reducing the Minimum Square Error (MSE) of $h(ss)$ calculated by Equation 6 using the measurement flow rate q and measurement value of h. Similarity, reduction of MSE between the $p_{out}^{(ss)}$ calculated (Equation 10) and the p_{out} measured adjusts m_1, m_2, y_0, and cv_0; and m_s, b_s and c_s adjustment is performed by MSE of measurement q and calculated $q^{(ss)}$ (Equation 14).

3.6 Model Predictive Control Formulation

The Non-linear Model Predictive Control (NMPC) is a regulatory problem that aims to maintain a setpoint of pump head h_r while minimizing the error between the setpoint and the actual value of h. The cost function C of NMPC is given

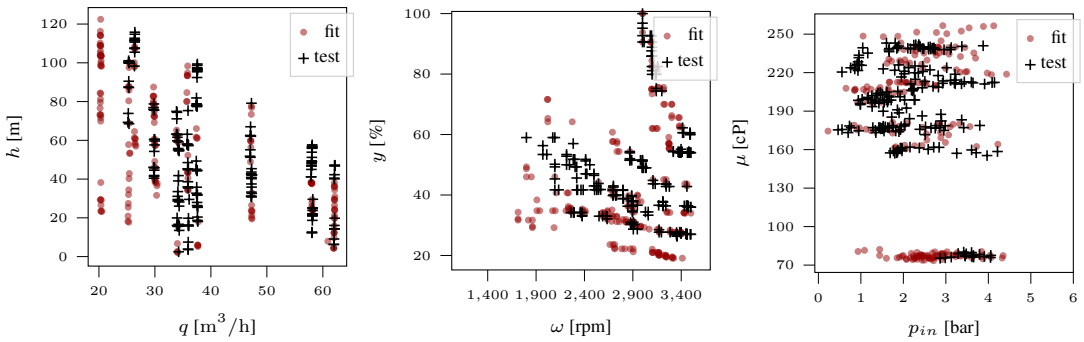

Figure 4: Fit and test distribution data

by

$$C = \int_0^T \left(\phi(h_r - h_{(t)})^2 + \left(\boldsymbol{u}_{(t)} - \boldsymbol{u}_{(t-dt)}\right)(1-\phi)\left(\boldsymbol{u}_{(t)} - \boldsymbol{u}_{(t-dt)}\right)^T\right)dt, \tag{18}$$

and considering discrete time step as

$$C \approx \sum_{k=0}^{T} \left(\phi(h_r - h_k)^2 + (\boldsymbol{u}_k - \boldsymbol{u}_{k-1})(1-\phi)(\boldsymbol{u}_k - \boldsymbol{u}_{k-1})^T\right)\Delta t. \tag{19}$$

Here, the ϕ parameter is a weighting parameter that avoids fluctuations in the manipulated variables y and ω.

The system is subject to a DDSM, SSM, and operational limits to ensure a safe operation. Operational limits correspond to the constraints:

- The choke valve opening being between 0-100% and the choke step being less than 2%;
- The ESP rotation is between 0-3500 rpm and the ESP step being less than 300 rpm;
- The input pressure is greater than 0 bar.

4. RESULTS AND DISCUSSIONS

The results obtained from the experiments are presented and discussed in this section. Table 2 shows the adjusted parameters for the reservoir model. Figure 5 shows the error of the ESP SSM prediction on the test dataset. It includes two subplots: the left subplot depicts the error of the ESP SSM prediction as a function of pump head h and pressure output p_{out}. In contrast, the right subplot shows the corresponding error distribution as a cumulative histogram.

Table 2: Adjusted Parameters.

Model	Parameters						Equation
ESP SSM	k_1 [m s^2]	k_2 [m^{-2}s^2]	k_3 [m^{-5}s^2]	k_4 [m^{-4}s^2]	k_5 [m^{-4}s^2]	n	6
	9.4000e-4	-7.6883e+0	2.8110e+5	5.1541e+6	1.1890e+6	6.5381e-1	
	m_1	m_2	y_0	cv_0 [m^2]			9
	7.1549e+0	1.2610e-3	5.5960e-1	5.2516e-2			
reservoir model	vc_s [m^3]	m_s [m^3 s]	b_s [m^4 s kg^{-1}]				11, 12
	1.3455e-4	3.7490e-13	2.7484e+10				
DSSM	a_{11}	a_{12} [m Pa^{-1}]	a_{21} [Pa m^{-1}]	a_{22}			15
	-7.6520e-2	2.8836e-7	-7.1212e+1	-3.1463e-2			
	b_{11}	b_{12} [m Pa^{-1}]	b_{21} [Pa m^{-1}]	b_{22}			15
	7.3870e-2	-9.9135e-8	9.5603e+1	2.9104e-2			

The h percent error decrease as the h increases, while p_{out} percent error presents values near the 5% in the interval between 4 and 10 bar — the cumulative histogram insights into the distribution of prediction errors. The horizontal axis represents the percentage of data, while the vertical axis represents the percent error. Each bar's height represents the data percentage with a percent error below the reference. The cumulative histogram (Fig. 5) reveals that at least 80% of

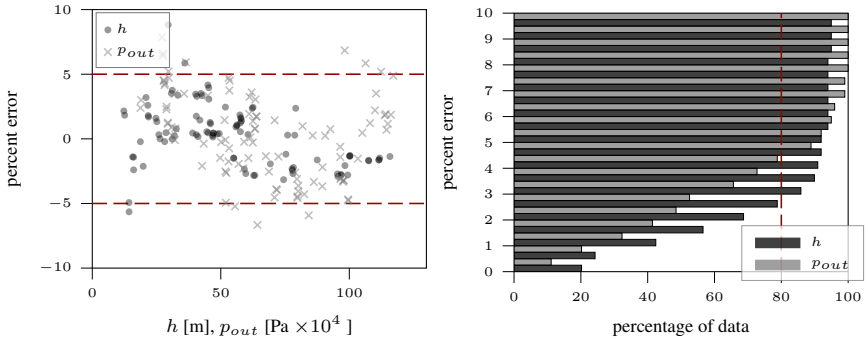

Figure 5: Percent error in ESP SSM prediction on test dataset

data have prediction errors below 3.5% and 5% for h and p_{out} predictions, respectively. Furthermore, nearly all the data, exhibit errors less than 8% for p_{out} predictions. The model performed well, with most data having relatively low errors.

Similarly, Figure 6 presents the error in reservoir model prediction on the test dataset to flow rate q predictions. The prediction errors decrease as the flow rate increases, indicating that the reservoir model's accuracy improves with higher flow rates. The cumulative histogram (Fig. 6) reveals that at least 80% of data have prediction errors below 0.3%. Furthermore, nearly all the data, close to 100%, exhibit errors of less than 0.5%. The flow rate prediction based on the pump oil's behavior is favorable because the pump is a positive-displacement pump.

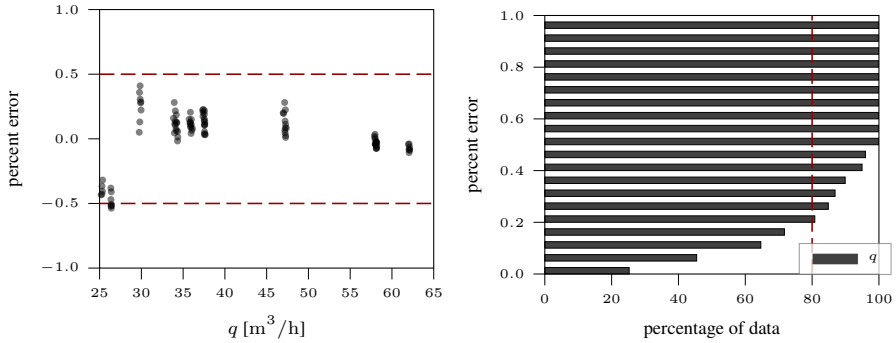

Figure 6: Percent error of reservoir model prediction on test dataset

The DSSM inputs are the steady-steady predictions of h and p_{out} and the DSSM outputs are the dynamical prediction of h and p_{out}. Figures 7 and 8 provide examples of the dynamic model prediction on the fit dataset and test dataset, respectively for a one-second prediction horizon.

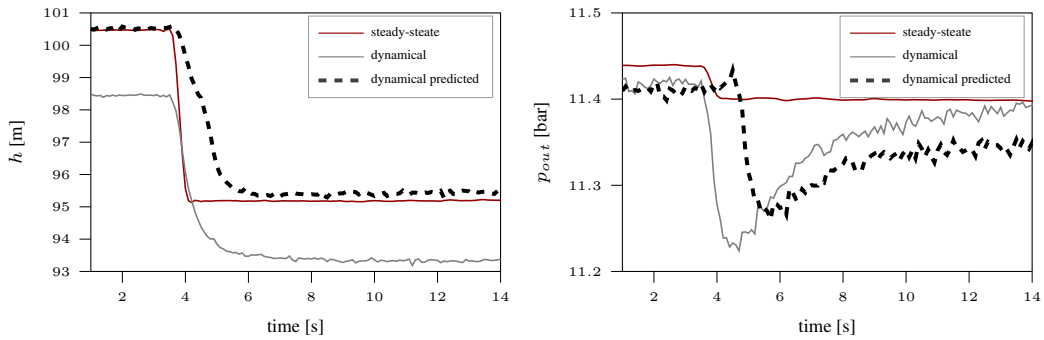

Figure 7: Example of dynamic model prediction on fit dataset

Figures 7 and 8 exhibits steady-state predictions in a red line, dynamical predictions in the black line, and real dynamical behavior in the gray line. Both, fit and test datasets exhibit a similar dynamical behavior between predictions and experimental values for h and p_{out}. h prediction exhibits a steady-state error between 1% and 4%, while p_{out} exhibits error below 1% (Fig. 7 and Fig.8). The dynamical has a delay in time near 0.5 [s], as expected. Generally dynamical model performs well in both, fit and test data. The steady-state percent error is more closely associated with the steady-state prediction that the dynamical model. An improvement in steady-state adjustment improved the overall model.

Figure 9 presents the percent error of the dynamic model prediction. Figure 9a shows the percent error on the fit dataset, while Fig. 9b displays the percent error on the test dataset. Figure 9a shows that at least 80% of data have

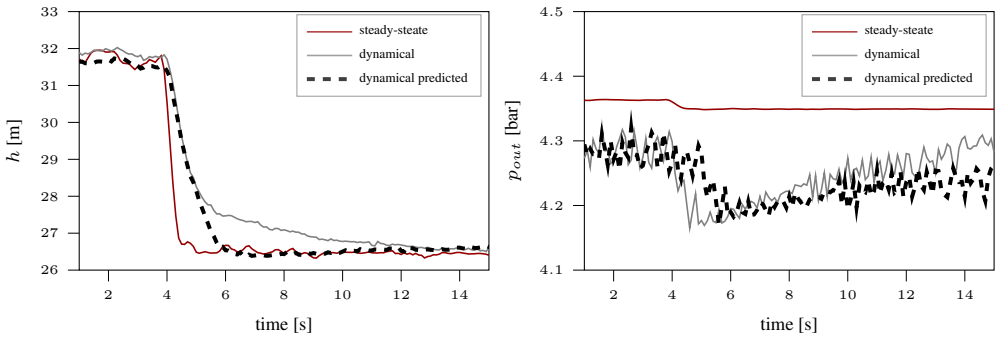

Figure 8: Example of dynamic model prediction on test dataset

prediction errors below 3.5% and 5.5% for p_{out} and h predictions, respectively, with the fit dataset. Figure 9b shows that at least 80% of data have prediction errors below 4% and 4.5% for p_{out} and h predictions, respectively. Model accuracy decreased a little for the test data. The dynamical model (Equation 15) adjusted well with most data, and the performance was well in the pump operation range.

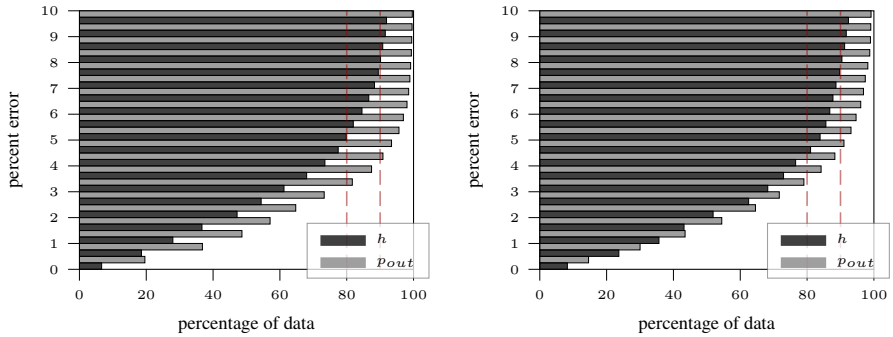

(a) Fit dataset (b) Test dataset

Figure 9: Percent error of dynamic model prediction

5. CONCLUSIONS

The model approach considered for NMPC was the Hammerstein-Wiener. The approach involved a steady-state model (ESP SSM) and a Dynamical State-Space (DSSM). The ESP SSM accounted for the ESP, choke valve, and upstream elements. The DSSM evaluates the variations in the pump head and output pressure. The proposed model showed good potential as an accurate and reliable control strategy for pump systems with non-linear dynamics.

The proposed model showed some divergence in steady-state and plant model values, which influence the dynamical behavior and predictions. As the steady-state model improves, the dynamical model improves significantly.

The non-linear MPC technique explored is a promissory regulatory control strategy in ESP and similar systems. The following steps consider testing the proposed model in an experimental bench and extending the methodology to multiphase flows considering apparent fluid viscosity.

6. ACKNOWLEDGMENTS

We acknowledge the support of the Energy Production Innovation Center (EPIC) at the University of Campinas (UNICAMP) and the financing by Equinor Brazil and the São Paulo Research Foundation (FAPESP, process 2019/10249-2). We acknowledge the support of Brazil's National Oil, Natural Gas, and Bio-fuels Agency (ANP) through the R&D levy regulation. We extend the recognition to the Center for Petroleum Studies (CEPETRO), the School of Mechanical Engineering (FEM), and the Artificial Lift and Flow Assurance Research Group (ALFA).

7. REFERENCES

Adesanwo, M., Bello, O., Zhu, D., Owen, B., Ogu, B., Ossai, J.C. and Iwo, G., 2019. "Interpreting downhole pressure and temperature data from ESP wells by use of inversion-based methods in samabri biseni field". In *Society of Petroleum Engineers - SPE Nigeria Annual International Conference and Exhibition 2019, NAIC 2019*. ISBN 9781613996911. doi:10.2118/198872-MS.

Biazussi, J.L., 2014. *Modelo de Deslizamento para Escoamento Gás-Liquido em Bomba Centrífuga Submersa Operando com Líquido de Baixa Viscosidade*. Ph.D. thesis, School of Mechanical Engeniering.

Bukhtoyarov, V.V., Tynchenko, V., Petrovskiy, E. and Buryukin, F., 2019. "Comparative Analisis of methos for simulating the well operation with electric submersible pump instalation". *Periódico Tchê Química*, Vol. 16, pp. 621–632.

Dazin, A., Caignaert, G. and Bois, G., 2007. "Transient behavior of turbomachineries: Applications to radial flow pump startups". *Journal of Fluids Engineering, Transactions of the ASME*, Vol. 129, No. 11, pp. 1436–1444. ISSN 00982202. doi:10.1115/1.2776963.

de Campos, M.C.M.M. and Teixeira, H.C.G., 2010. *Controles Típicos de Equipamentos e Processos Industriais*. Editora Blucher, 1st edition. ISBN 9788521203988.

De Delou, P.A., De Azevedo, J.P., Krishnamoorthy, D., De Souza, M.B. and Secchi, A.R., 2019. "Model predictive control with adaptive strategy applied to an electric submersible pump in a subsea environment". *IFAC-PapersOnLine*, Vol. 52, No. 1, pp. 784–789. ISSN 24058963. doi:10.1016/j.ifacol.2019.06.157. URL https://doi.org/10.1016/j.ifacol.2019.06.157.

Denney, T., Wolfe, B. and Zhu, D., 2013. "Benefit Evaluation of Keeping an Integrated Model During Real-Time ESP Operation". In *2013 SPE Digital e Energy Conference and Exhibition held in The e Woodlands*. Texas, USA, p. 13.

Greblicki, W. and Pawlak, M., 1986. "Identification of Discrete Hammerstein Systems Using Kernel Regression Estimates". *IEEE Transactions on Automatic Control*, Vol. 31, No. 1, pp. 74–77. ISSN 15582523. doi:10.1109/TAC.1986.1104096.

Greblicki, W. and Pawlak, M., 1994. "Dynamic System Identification with Order Statistics". *IEEE Transaction on Information Theory*, Vol. 40, No. 5, pp. 1474–1489.

Janevska, G., 2013. "Mathematical Modeling of Pump System". *Electronic International Interdisciplinary Conference*, Vol. 2, pp. 455–458. URL http://www.eiic.cz/archive/?vid=1&aid=3&kid=20201-50&q=f6.

Jimenez, G.E.C., 2019. *Controle Especialista Aplicado ao Bombeio Centrífugo Submerso*. Ph.D. thesis, Universidad Estadual de Campinas. URL http://www.repositorio.unicamp.br/handle/REPOSIP/342414.

Jimenez, G.E.C., Ricardo, D.M.M. and Ferreira, J.V., 2016. "Nonlinear Modeling of an Electric Submersible Pump Operating with Multiphase Flow by SVMr and Genetic Algorithms". *International Journal of Scientific Research and Innovative Technology*, Vol. 3, No. 4, pp. 27–42.

Karassik, I.J., Krutzsh., W., Fraser, W.H. and Messina, J.P., 1976. *Pump Handbook.* Number (1) in 1. McGRAW-HILL, 1st edition. ISBN 0070340323.

Krishnamoorthy, D., Bergheim, E.M., Pavlov, A., Fredriksen, M. and Fjalestad, K., 2016. "Modelling and Robustness Analysis of Model Predictive Control for Electrical Submersible Pump Lifted Heavy Oil Wells". *IFAC-PapersOnLine*, Vol. 49, No. 7, pp. 544–549. ISSN 24058963. doi:10.1016/j.ifacol.2016.07.399. URL http://dx.doi.org/10.1016/j.ifacol.2016.07.399.

Kullick, J. and Hackl, C.M., 2017. "Dynamic modeling and simulation of deep geothermal electric submersible pumping systems". *Energies*, Vol. 10, No. 10. ISSN 19961073. doi:10.3390/en10101659.

Lastra, R., 2019. "Electrical submersible pump digital twin, the missing link for successful condition monitoring and failure prediction". In *Society of Petroleum Engineers - Abu Dhabi International Petroleum Exhibition and Conference 2019, ADIP 2019*. ISBN 9781613996720. doi:10.2118/197156-ms.

Pavlov, A., Krishnamoorthy, D., Fjalestad, K., Aske, E. and Fredriksen, M., 2014. "Modelling and model predictive control of oil wells with electric submersible pumps". In *2014 IEEE Conference on Control Applications, CCA 2014*. pp. 586–592. ISBN 9781479974092. doi:10.1109/CCA.2014.6981403.

Pineda, L.F.R., 2016. *Controle do Ponto de Operação de Bombas Centrífugas Submersas em Escoamento Líquido-Gás Usando Redes Neurais*. Master's thesis, University of Campinas.

Ricardo, D.M.M., Jiménez, G.E.C., Ferreira, J.V. and Meirelles, P.S., 2018. "Multiphase gas-flow model of an electrical submersible pump". *Oil and Gas Science and Technology*, Vol. 73. ISSN 19538189. doi:10.2516/ogst/2018031.

Robert W. Fox, Philip J. Pritchard and Alan T. McDonald, 2020. *Introduction to Fluid Mechanics*. 10. John Wiley & Sons, 10th edition. ISBN 978-1-119-61649-8.

Saito, S., 1982. "The Transient Characteristics of a Pump during Start Up". *Bulletin of the JSME*, Vol. 25, No. 201, pp. 372–379.

Thornhill, D.G., Zhu, D. and Incorporated, B.H., 2009. "Fuzzy Analysis of ESP System Performance". In *SPE Annual Technical Conference and Exhibition*. SPE, New Orleans, Louisiana, USA. ISBN 9781555632632. doi:10.2118/123684-MS.

Thorsen, O.V. and Dalva, M., 2001. "Combined electrical and mechanical model of electric submersible pumps". *IEEE Transactions on Industry Applications*, Vol. 37, No. 2, pp. 541–547. ISSN 00939994. doi:10.1109/28.913720.

8. RESPONSIBILITY NOTICE

The authors are solely responsible for the printed material included in this paper.